

OPEN

Computational Studies on the Thermodynamic and Kinetic Parameters of Oxidation of 2-Methoxyethanol Biofuel via H-Atom Abstraction by Methyl Radical

Mohamed A. Abdel-Rahman¹, Tarek M. El-Gogary^{2,3,4}, Nessreen Al-Hashimi^{5*}, Mohamed F. Shibl⁵, Kazunari Yoshizawa⁶ & Ahmed M. El-Nahas^{1*}

In this work, a theoretical investigation of thermochemistry and kinetics of the oxidation of bifunctional 2-Methoxyethanol (2ME) biofuel using methyl radical was introduced. Potential-energy surface for various channels for the oxidation of 2ME was studied at density function theory (M06-2X) and *ab initio* CBS-QB3 levels of theory. H-atom abstraction reactions, which are essential processes occurring in the initial stages of the combustion or oxidation of organic compounds, from different sites of 2ME were examined. A similar study was conducted for the isoelectronic *n*-butanol to highlight the consequences of replacing the Υ CH₂ group by an oxygen atom on the thermodynamic and kinetic parameters of the oxidation processes. Rate coefficients were calculated from the transition state theory. Our calculations show that energy barriers for *n*-butanol oxidation increase in the order $\alpha < \text{O} < \Upsilon < \beta < \xi$, which are consistent with previous data. However, for 2ME the energy barriers increase in the order $\alpha < \beta < \xi < \text{O}$. At elevated temperatures, a slightly high total abstraction rate is observed for the bifunctional 2ME (4 abstraction positions) over *n*-butanol (5 abstraction positions).

Social turning to green (eco-friendly) energy sources which are accompanied with minimum quantities of gases emission became an inevitable matter and cannot be ignored particularly with rising world energy demand, high price, and global environmental degradation^{1,2}. Unifunctional alcohol, *n*-butanol, is produced directly from the fermentation of cellulosic biomass³⁻⁶ and characterized by high energy content, low vapor pressure, less corrosive than bioethanol, and can be blended with gasoline⁷. *n*-Butanol burning properties as biofuel and/or biofuel additive was being a subject of many experimental reports^{6,8-22} in different engine systems. Regarding bifunctional compounds, many effective chemical techniques were proposed for the conversion of different biomass forums to high yielded diol compounds²³⁻²⁹. Ethylene glycol (EG) with the dihydroxy group is known as a coolant viscous liquid for automobile engines with serious defects that prevent its use in a pure form such as high toxicity, hydrophobicity, and low internal energy³⁰. Modification of EG with alkyl group alters the overall chemical and physical properties of original biofuel such as decrease viscosity, water absorption, toxicity, increase carbon content, and miscibility in oils.

Using bifunctional 2-methoxyethanol (2ME) as biofuel may be more suiting current engine infrastructure since the former is characterized by its high internal energy (nearly equal butanol isomers), low water absorbability, low

¹Chemistry Department, Faculty of Science, Menoufia University, Shebin El-Kom, Egypt. ²Chemistry Department, Faculty of Science, Jazan University, 2097, Jazan, Kingdom of Saudi Arabia. ³School of Allied Health Sciences, Faculty of Health and Life Sciences, DeMontfort University, Leicester, UK. ⁴Chemistry Department, Faculty of Science, Damietta University, New Damietta, Egypt. ⁵Department of Chemistry and Earth Sciences, College of Arts and Sciences, Qatar University, P.O. Box 2713, Doha, Qatar. ⁶Institute for Materials Chemistry and Engineering and IRCCS, Kyushu University, Fukuoka, 819-0395, Japan. *email: nalem@qu.edu.qa; amelnahas@hotmail.com

vapor pressure, and expected oxidations readily with different radicals in atmospheric and combustion regimes. Methyl radical is one of the most important oxidizing fragments which can exist in automotive engines during initiation processes. At high-temperature regime, H-atom abstraction of biofuels is considered as the main contributors to the total rate of fuel combustion. Experimentally, a few studies were proposed to measure the rate constants of bimolecular reactions of $\bullet\text{OH}$ radical with series of hydroxyl ether compounds including 2ME using various chemical techniques like flash photolysis resonance fluorescence (FPRF)³¹, pulse laser photolysis resonance fluorescence³², and gas chromatography with flame ionization detection (GC-FID)³³. Stemmler *et al.*³⁴ calculated the rate coefficient of 2ME and 2-ethoxyethanol (2EE) using the rate constant of heptanol and hexanol at room temperature.

Galano *et al.*³⁵ performed a computational study on the oxidation of the $\bullet\text{OH}$ radical with series of branched hydroxyl ethers including 2ME at the CCSD(T)/6-311 G++(d,p)//B3LYP/6-311 G++(d,p) level of theory. They discussed branching ratios at thermal temperature, calculated Arrhenius parameters in the range of temperature 250–440 K, and emerged the effect of H-bond formation with the etheric O-atom upon the abstraction mechanism and transition states formations.

On the other side, the bimolecular oxidation of *n*-butanol with different oxidizing agents like $\bullet\text{OH}$,^{36–39} $\bullet\text{HO}_2$,^{39–41} and $\bullet\text{CH}_3$ radical^{42,43} received a lot of attention. The closest studies to the current work on *n*-butanol were performed by Katsikadakis *et al.*^{42,43}. They estimated barrier energies at different *ab initio* levels⁴² and rate constants of *n*-butanol oxidation with $\bullet\text{CH}_3$ radical⁴³ in a temperature range of 500–2000 K using CCSD(T)/CBS energies. They found high competition of α and γ channels during the applied temperature. In the current study, we will re-investigate their work at a high *ab initio* CBS-QB3 level and compare with 2ME data to shed some light on the main thermodynamic and kinetic consequences of the presence of an electro-donner (hetero) atom instead of the methyl group.

Computational Details

All calculations were carried out using Gaussian-16W program⁴⁴. Geometry optimizations of reactants, transition states, and products have been performed using Density function theory (DFT) Minnesota M06-2X hybrid meta functional with 54% HF exchange⁴⁵ with the 6-31 + G(d, p) basis set. M06-2X function was designed by Zhao *et al.*⁴⁵ to give accurate thermokinetic calculations and tested in many advanced publications^{46–50}. The high *ab initio* CBS-QB3^{51–53} method was also used for providing accurate energies at low computational cost. The CBS-QB3 methodology includes geometry optimization and frequency calculation at the B3LYP/6-311 G(d, p) level followed by CCSD(T)/6-31 + G(d), MP4SDQ/6-31 + G(d, p), and MP2/6-311 + G(2df, 2p) single point energy calculations with CBS extrapolation. Transition states for H-atom abstraction pathways were located using the eigenvector-following (EF) optimization technique which is implemented in the Gaussian suit of programs. Linear Synchronous Transit (LST) method is used to search for the saddle point (maximum energy) on the linear path between reactants and products. Synchronous Transit-Guided Quasi-Newton (STQN)^{54,55} method is a techniques of Synchronous transit (ST) methods that use the quadratic synchronous transit (QST) approach which chooses the intermediate point in a perpendicular direction to the LST trajectory to get closer to the quadratic region of the transition state then uses a quasi-Newton or eigenvector-following algorithm to complete the optimization process. The STQN methods can be obtained by invoked keywords QST2 which requires input file contain two molecule specifications of the reactant and product, and QST3 that requires three molecule specifications of the reactant, the product, and an initial structure for the transition state. For accurate transition state location, the STQN methods^{54,55} (QST2 and QST3 keywords) were used to check the efficiency of that obtained by Berny algorithm (OPT = TS). Vibrational frequency calculations were conducted at the same level of theory to characterize the nature of those points as minima (real frequencies) or transition state (only one imaginary frequency) and to correct energies for zero-point (ZPE) and thermal contributions at 298 K. Vibrational modes of different structures were visualized using the ChemCraft program⁵⁶. For step by step verifying of transition states existence, the reactants connected with desired products minimum energy paths (MEP) were computed through intrinsic reaction coordinates(IRC)^{57,58} at M06-2X/6-31 + G(d, p).

The highly accurate kinetic program Kisthelp⁵⁹ was used for rate constants (k) calculations of chemical reactions over 200–2000 K using Classical transition state theory⁶⁰ and Wigner correction⁶¹ as follows:

$$k_{(T)}^{\text{TST}} = \sigma \frac{k_B T}{h} \left(\frac{RT}{P^\circ} \right)^{\Delta n} e^{-\Delta^\ddagger G^\circ(T)/k_B T} \quad (1)$$

where k_B , h , R , and T are Boltzmann, Planck, ideal gas constant, and the system's temperature in Kelvin, respectively; σ is the reaction path degeneracy; P° is the standard pressure = 1 atm; $\Delta^\ddagger G^\circ(T)$ is the standard Gibbs free energy of activation for reaction, while Δn can takes integer values zero for unimolecular decomposition and one for bimolecular oxidation.

To account for tunneling effects, the transmission coefficient $\chi(T)$ along the reaction coordinate and, thus, the rate constant $k_{\text{TST/W}}(T)$ including tunneling correction is given by

$$k_{\text{TST/W}}(T) = \chi(T)k_{\text{TST}}(T)$$

The transmission coefficient $\chi(T)$ was calculated using the Wigner correction⁶¹ which is the simplest form and assumes a parabolic potential for the nuclear motion near the transition state. The Wigner transmission coefficient is given by

$$\chi(T) = 1 + 1/24 [h\nu/k_B T]^2$$

where ν is the imaginary frequency of the transition state.

Conformer	CBS-QB3	G3
tGg-	0.00	0.00
gGg-	1.57	1.52
tTt	2.61	2.57
tTg	2.75	2.64
tGt	2.86	2.91
tGg	3.20	3.23
g-Gt	3.26	3.30
g-Gg	3.77	3.75
gTt	4.09	3.99
gTg-	4.14	3.96
gTg	4.36	4.20
gGt	4.38	4.38

Table 1. Relative energies (ΔE_0 , kcal/mol) of 2ME conformers at CBS-QB3 and G3.

Tukey honestly significant difference⁶² (Tukey HSD) is a statistical method which is used to find whether the relation between two groups is significantly different or not. Tukey criterion (T) can be obtained from the formula

$$T = q_{\alpha(c,n-c)} \sqrt{\frac{MSE}{n_i}}$$

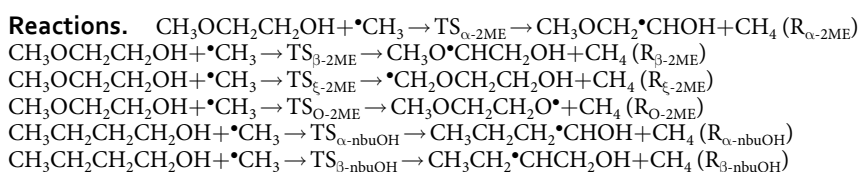
where $q_{\alpha(c,n-c)}$ is studentized range distribution based on the degree of freedoms (df) of c (number of columns), n is total sample size, MSE is the mean square error which is obtained from the analysis of the variance “ANOVA” table, and n_i is the sample size in a specific column with the smallest number of observation.

Results and Discussion

Both of *n*-butanol and 2ME have three main dihedral angles which, in case of *n*-butanol and 2ME (in parentheses), are $C_\xi - C_T - C_\beta - C_\alpha$ ($C_\xi - O_\beta - C_\beta - C_\alpha$), $C_T - C_\beta - C_\alpha - O_\alpha$ ($O_\beta - C_\beta - C_\alpha - O_\alpha$), and $C_\beta - C_\alpha - O_\alpha - H$ ($C_\beta - C_\alpha - O_\alpha - H$). Each dihedral angle can be exist in trans (T, t), gauche (G, g) or anti-gauche (G-, g-) form. *n*-Butanol conformations were being a subject for many past discussions at different levels of theory^{41,42,63,64}. Results confirmed the existence of fourteen conformers of *n*-butanol with a relatively high stability of tGt conformer with narrowed energy range ≤ 2 kcal/mol at the G3⁴¹ and CBS-QB3⁶³ methods. Our results of conformational analysis of 2ME are tabulated in Table 1, where two computational methods are used to calculate the relative conformer energies. The most stable conformer is tGg- with an intramolecular hydrogen bond (2.329 Å, see Table S1 in the SI file), which lies below the least stable conformer, gGt, by 4.38 kcal/mol. The next most stable conformer is gGg- which is less than 2 kcal/mol (Table 1) above the global minimum structure. Our results at CBS-QB3 and G3 are in good agreement with the reported data of 2ME conformers stability⁶⁵. The higher stability of tGg- conformers enhanced its high yield at different combustion temperature in contrast to *n*-butanol. Optimization and energies of different 2ME conformers are presented in the Supporting Information (SI). Our study will be conducted on the most stable structures tGt, tGg- for *n*-butanol and 2ME, respectively at CBS-QB3.

Figure 1 shows bond dissociation energies (BDEs) of *n*-butanol (tGt), 2ME (tGg-) at 298 K and their optimized structures at CBS-QB3. The results obtained for tGt conformer *n*-butanol are in good agreement with literatures^{9,12} and our previous results⁶⁶ at the same level. From Fig. 1, it is obvious that $C_\beta - C_T$ (*n*-butanol) and $C_\beta - O_\beta$ (2ME) have nearly equal bond energies of 90.3 and 90.0 kcal/mol, respectively. The O-H bond has the highest bond energy in the two compounds with the values of 105.3 and 108.2 kcal/mol for *n*-butanol and 2ME, respectively. The $C_\alpha - H$ bonds have the weakest bond energies among different abstraction positions with 95.6 kcal/mol for *n*-butanol and 96.2 kcal/mol for 2ME. Replacing C_T with O_β lowers bonds energies for $C_\beta - H$ and $C_\xi - H$ with 4.0 and 4.4 kcal/mol, respectively. For bifunctional 2ME, H-atom abstraction from α and β positions is easier and faster compared to the ξ position. This trend could be explained by the effect of the adjacent two active groups⁶⁷.

Based on similar studies of Katsikadacos *et al.*^{42,43} for *n*-butanol oxidation and by comparing all transition states for different H-abstractions from the same site (see SI Tables S3 and S4). The results indicated that all hydrogen atoms linked to the same carbon atom can be considered equivalent; the notations of carbon atoms are named relative to the alcoholic oxygen. *n*-Butanol has five abstraction sites α , β , γ , ξ , and alcoholic hydrogen. These formed radicals are $CH_3CH_2CH_2\cdot CHOH$, $CH_3CH_2\cdot CHCH_2OH$, $CH_3\cdot CHCH_2CH_2OH$, $\cdot CH_2CH_2CH_2CH_2OH$, and $CH_3CH_2CH_2CH_2O\cdot$, while 2ME has only four abstraction sites α , β , ξ , and alcoholic hydrogen producing $CH_3OCH_2\cdot CHOH$, $CH_3O\cdot CHCH_2OH$, $\cdot CH_2OCH_2CH_2OH$, and $CH_3OCH_2CH_2O\cdot$. The investigated reaction channels are summarized as follows:



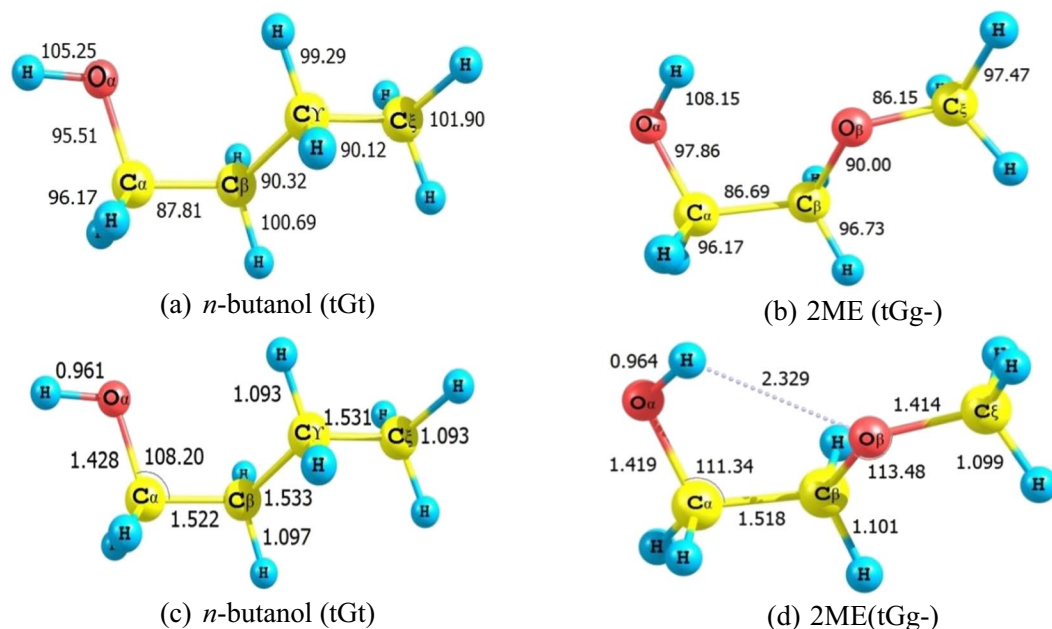
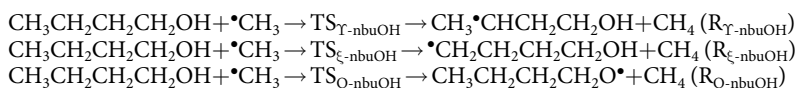


Figure 1. Bond dissociation energies (kcal/mol) of (a) *n*-butanol (tGt), (b) 2ME (tGg-) at 298 K and optimized structures of (c) *n*-butanol (tGt), (d) 2ME (tGg-) at B3LYP/6-311 G(d, p) (a part of CBS-QB3 method).



Optimized structures of transition states for H-atom abstraction from 2ME (tGg-) and *n*-butanol (tGt), by the $\bullet\text{CH}_3$ radical are displayed in Fig. 2. For *n*-butanol, α transition state proceeds through stretching the broken $\text{C}_\alpha\text{-H}$ bond by 17.1% and elongation of the formed $\text{C}_{\text{methyl}}\text{-H}$ bond by 33.3% relative to reactants and products, respectively. The bond breaking/bond forming of the other transition states $\text{TS}_{\beta\text{-nbuOH}}$, $\text{TS}_{\text{T-nbuOH}}$, $\text{TS}_{\xi\text{-nbuOH}}$, and $\text{TS}_{\text{O-nbuOH}}$ are 20/28.4%, 20.2/27.7%, 21.2/27%, and 24.6/19.9%, respectively. For 2ME, bond breaking/bond forming are 17.2 / 32.7%, 18/ 32.3%, 18.7/31.1%, and 25.8/18.9% for $\text{TS}_{\alpha\text{-2ME}}$, $\text{TS}_{\beta\text{-2ME}}$, $\text{TS}_{\xi\text{-2ME}}$, and $\text{TS}_{\text{O-2ME}}$, respectively. The calculated data are consistent with the Hammond postulate⁶⁸ which stated that for exothermic reactions, the transition state structure and energy are close to reactants rather than products, while for endothermic reactions (alcoholic H-atom abstraction), the structure and energy of the transition state are close to products rather than reactants.

Tables 2, 3 summarize energy barriers and reaction energies for the bimolecular oxidation of *n*-butanol, and 2ME with methyl radical calculated at different levels of theory. We have recalculated the energy barriers for the oxidation of *n*-butanol with methyl radical at CBS-QB3 to compare 2ME at the same level of theory. Comparing the obtained transition states for H-atom abstraction from α and β sites for 2ME and *n*-butanol by Berny algorithm with that of STQN methods indicated that the obtained transition states from the two methods are similar (barrier height difference is less than 0.1 kcal/mol). So the calculations based on Berny algorithm (OPT = TS) can give accurate barrier heights.

For *n*-butanol, the estimated barrier energies at CBS-QB3 agree well with the reported data at ROCBS-QB3⁴² with very small energy differences being maximum for Υ channel of 0.6 kcal/mol. Our results at CBS-QB3 illustrate less agreement with CCSD(T)/CBS⁴³ having the highest energy difference of 1.9 kcal/mol for H-atom abstraction from oxygen. For 2ME, the β and ξ products are much stable relative to those of *n*-butanol due to the ability to form a delocalized π bond with a lone pair of etheric oxygen. The results of M06-2X are in good agreement with that obtained using the acceptable CBS-QB3 level. From Tables 3 and S7, the computed reaction energies and enthalpies for *n*-butanol and 2ME at CBS-QB3 and M06-2X /6-31 + G(d, p) suggest that all hydrogen atom abstraction channels from the carbon atoms are exothermic processes and only the abstraction reaction from the oxygen atom is endothermic. The most exothermic process is the α hydrogen atom abstraction and the least exothermic one is the H-atom abstraction from ξ position for both compounds at the two computational methods. The potential energy diagram of 2ME oxidation by $\bullet\text{CH}_3$ radical at CBS-QB3 appears in Fig. 3.

The calculated barrier heights order of 2ME oxidation is consistent with the corresponding product radical stability. α H-atom abstraction represents the most preferable decomposition pathway both thermodynamically and kinetically with barrier energy of 10.1 kcal/mol and reaction energies of -9.7 and -9.3 kcal/mol for *n*-butanol and 2ME, respectively. All channels are exothermic, except that of alcoholic H-abstraction with reaction energies of 0.1 and 2.6 kcal/mol for *n*-butanol and 2ME, respectively, at CBS-QB3. Alcoholic H-abstraction pathway is more kinetically preferable for *n*-butanol oxidation compared to that for 2ME. This could be easily understood on the basis of intramolecular hydrogen bond formation in 2ME. Table 4 presents enthalpies of formation of radicals derived from *n*-butanol and 2ME oxidation and their stabilities relative to the least stable

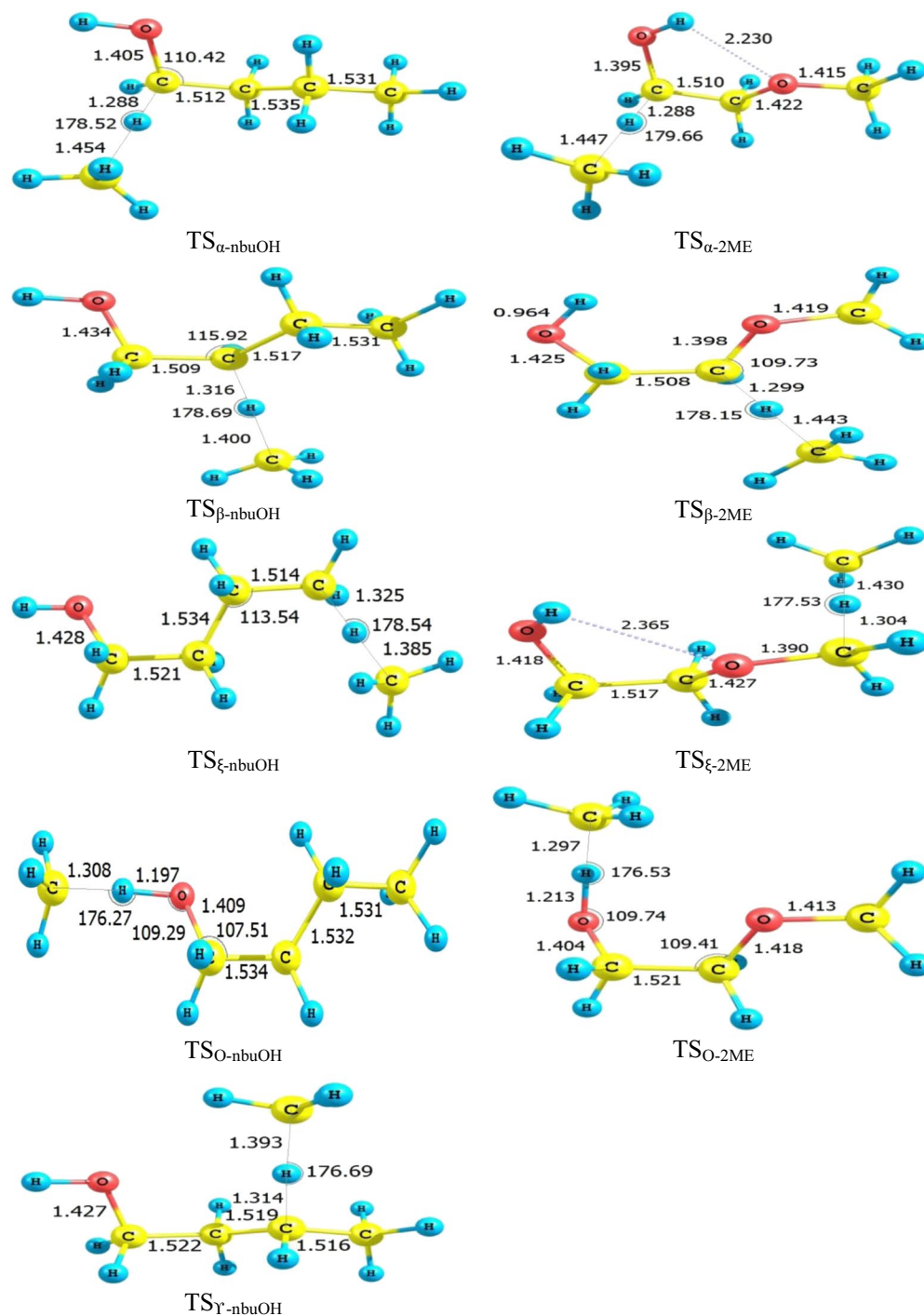


Figure 2. Optimized structures of transition states at B3LYP/6–311 G(d, p) (a part of CBS-QB3 method).

n-butoxy radical $\text{CH}_3\text{CH}_2\text{CH}_2\text{CH}_2\text{O}^\bullet$ and methoxyethoxy radical, $\text{CH}_3\text{OCH}_2\text{CH}_2\text{O}^\bullet$, respectively. According to Table 4, the calculated enthalpies of formation for n-butanol and its radicals are in an excellent agreement with theoretical values obtained by Black *et al.*⁹ and with the available experimental results.

Estimation of ionization energies (IE) and electron affinities (EA) for chemical compounds are a crucial step for the determination of many chemical properties such as softness, hardness, electronegativity and the chemical potential^{69,70}. IEs and EAs of n-butanol, 2ME, and their radicals calculated theoretically using the adiabatic and vertical approaches at CBS-QB3 level and the available experimental data are presented in Table 5. For further confirmation of the accuracy of our theoretical calculations at CBS-QB3 level, the Enthalpies of formation (AE) and adiabatic ionization energies (AIEs) for a group of oxygenated compounds which previously experimentally detected are collected in Table 6, while Table 7 tests the theoretically estimated barrier heights against the experimental activation energy (E_a) for their reaction with methyl radical.

Site	<i>n</i> -butanol			2ME	
	CCSD(T)/CBS ^a	ROCBS-QB3 ^b	CBS-QB3 ^c	CBS-QB3 ^c	M06-2X/6-31 + G(d, p) ^c
α	11.11	10.11	10.12	10.11	9.45
β	12.73	11.59	11.95	10.39	9.64
γ	12.30	11.25	11.86	—	—
ξ	14.41	13.57	13.64	11.80	10.84
O	12.88	10.70	10.99	11.86	10.87

Table 2. Barrier heights (E_0^\ddagger , kcal/mol) for H-atom abstraction from *n*-butanol (tGt) and 2ME (tGg-) by the $\bullet\text{CH}_3$ radical at different levels of theory. ^aRef.⁴³, ^bref.⁴², and ^ccurrent study.

Site	<i>n</i> -butanol			2ME	
	CCSD(T)/CBS ^a	ROCBS-QB3 ^b	CBS-QB3 ^c	CBS-QB3 ^c	M06-2X/6-31 + G(d, p) ^c
α	-9.32	-9.72	-9.72	-9.30	-9.38
β	-4.59	-4.83	-4.86	-8.97	-8.49
γ	-5.88	-6.19	-6.21	—	—
ξ	-3.42	-3.56	-3.59	-8.03	-7.56
O	0.91	0.14	0.13	2.64	1.50

Table 3. Reaction energies (E_0 , kcal/mol) for H-atom abstraction from *n*-butanol (tGt) and 2ME (tGg-) by the $\bullet\text{CH}_3$ radical at different levels of theory. ^aRef.⁴³, ^bref.⁴², and ^ccurrent study.

Species	AE	Exp.	ΔE	Species	AE	Exp.	ΔE
$\text{CH}_3\text{CH}_2\text{CH}_2\text{CH}_2\text{OH}$	-66.05	-65.7 ^a	—	$\text{CH}_3\text{OCH}_2\text{CH}_2\text{OH}$	-91.29	-90.04 ± 1.94 ^c , -94.58 ^d	—
$\text{CH}_3\text{CH}_2\text{CH}_2\text{CH}_2\text{O}^\bullet$	-13.10	-14.7 ^b	0	$\text{CH}_3\text{OCH}_2\text{CH}_2\text{O}^\bullet$	-35.26	—	0
$\bullet\text{CH}_2\text{CH}_2\text{CH}_2\text{CH}_2\text{OH}$	-16.26	—	-3.16	$\bullet\text{CH}_2\text{OCH}_2\text{CH}_2\text{OH}$	-45.91	—	-10.68
$\text{CH}_3\text{CH}_2\bullet\text{CHCH}_2\text{OH}$	-17.46	—	-4.36	$\text{CH}_3\text{O}^\bullet\text{CHCH}_2\text{OH}$	-46.67	—	-11.61
$\text{CH}_3\text{CH}_2\text{CH}_2\bullet\text{CHOH}$	-22.58	—	-9.48	$\text{CH}_3\text{OCH}_2\bullet\text{CHOH}$	-47.22	—	-11.95
$\text{CH}_3\bullet\text{CHCH}_2\text{CH}_2\text{OH}$	-18.86	—	-5.76	—	—	—	—

Table 4. Enthalpies of formation using atomization energy approach (AE, $\Delta H_{f,298}$), and relative radicals' stabilities (ΔE) derived from *n*-butanol and 2ME (kcal/mol) at CBS-QB3. ^aRef.⁷¹, ^bref.⁷², ^cref.⁷³, ^dref.⁷⁴.

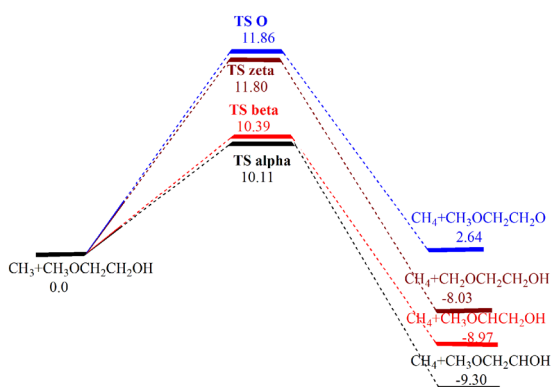


Figure 3. Potential energy diagram (E_0^\ddagger , E_0 , kcal/mol) of H-atom abstraction from 2ME by the $\bullet\text{CH}_3$ radical at CBS-QB3.

The obtained results in Tables 4–7 show a good agreement between the theoretical values of AE, IE, EA, and E_a and the available experimental data indicating the suitability of the employed level of theory.

Tukey test is used to examine the difference between theoretical and experimental results presented in Table 6. Our results (Table S8) reveal that the absolute difference between the averages of the experimental and theoretical data $|\bar{X}_{\text{exp.}} - \bar{X}_{\text{theo.}}|$ is 0.53 which is less than T of 129 indicating a high constancy between the theoretical and experimental results.

Branching ratio analysis of *n*-butanol (Table S11) indicates domination of α abstraction with around 16% contribution of the alcoholic H-atom abstraction at temperature up to 500 K. At $T > 500$ K, the contribution of the γ channel increases with the decline of contribution from α and alcoholic channels. At high temperature (T

Species	AIEs	VIEs	IE. Exp.	AEAs	VEAs	EA. Exp.
CH ₃ CH ₂ CH ₂ CH ₂ OH	228.12	241.85	232.3 ± 1.15 ^a , 229.77 ± 1.15 ^b , 244.72 ± 1.61 ^c , 232.07 ± 0.46 ^d , 238.51 ^{e,f} , 230.92 ^g , 239.89 ^h , 240.12 ± 0.69 ⁱ	-17.97	-14.97	—
CH ₃ OCH ₂ CH ₂ OH	218.19	239.18	232.99 ^j	-14.71	-13.65	—
CH ₃ CH ₂ CH ₂ CH ₂ O [*]	225.71	233.36	212.06 ± 1.15 ^k	42.41	38.89	43.7 ± 2.3 ^k , 40.94 ± 2.3 ^l , 41.4 ± 2.99 ^m , 20.44 ⁿ
[*] CH ₂ CH ₂ CH ₂ CH ₂ OH	155.51	189.57	—	4.56	26.82	—
CH ₃ CH ₂ [*] CHCH ₂ OH	167.87	180.70	—	7.03	0.10	—
CH ₃ CH ₂ CH ₂ [*] CHOH	151.39	168.23	—	-1.05	-12.17	—
CH ₃ [*] CHCH ₂ CH ₂ OH	166.71	175.66	—	35.89	-8.06	—
CH ₃ OCH ₂ CH ₂ O [*]	215.21	238.13	—	101.89	138.41	—
[*] CH ₂ OCH ₂ CH ₂ OH	89.29	119.54	—	5.20	-7.44	—
CH ₃ O [*] CHCH ₂ OH	151.38	175.53	—	9.10	-3.00	—
CH ₃ OCH ₂ [*] CHOH	150.98	171.85	—	2.31	-12.32	—

Table 5. The computed values of adiabatic ionization energies (AIEs), vertical ionization energies (VIEs), adiabatic electron affinities (AEAs), and vertical electron affinities (VEAs), in kcal/mol, for *n*-butanol, 2ME, and their radicals at CBS-QB3 level. ^aRef.⁷⁵, ^bref.⁷⁶, ^cref.⁷⁷, ^dref.⁷⁸, ^eref.⁷⁹, ^fref.⁸⁰, ^gref.⁸¹, ^href.⁸², ⁱref.⁸³, ^jref.⁸⁴, ^kref.⁸⁵, ^lref.⁸⁶, ^mref.⁸⁷, ⁿref.⁸⁸.

Species	AE	AE. Exp.	AIEs	IE. Exp.
CH ₃ OH	-48.87	-48.20 ^a	252.12	252.31 ± 0.69 ^d
CH ₃ CH ₂ OH	-56.64	-56.10 ^a	243.38	244.72 ^c
CH ₃ CH ₂ CH ₂ OH	-61.10	-60.90 ^a	241.19	241.96 ± 0.69 ^d
CH ₃ CH ₃	-20.18	-20.03 ± 0.07 ^b	268.97	266.11 ^f
CH ₃ OCH ₃	-45.39	-44.00 ± 0.12 ^c	231.12	230.58 ± 0.58 ^g
CH ₃ OCH ₂ CH ₃	-54.03	-51.70 ± 0.16 ^c	221.36	223.56 ± 1.61 ^h

Table 6. Enthalpies of formation (AE) and adiabatic ionization energies (AIEs) for some oxygenated compounds (kcal/mol) at CBS-QB3. ^aRef.⁷¹, ^bref.⁸⁹, ^cref.⁹⁰, ^dref.⁸³, ^eref.⁹¹, ^fref.⁹², ^gref.⁹³, ^href.⁷⁷.

Species/site	α	E _a . Exp.	β	E _a . Exp.	O	E _a . Exp.
CH ₃ OH	12.39	10.40 ^a	—	—	10.94	6.40 ^a
CH ₃ CH ₂ OH	10.28	9.70 ^b	14.95	—	10.91	9.39 ^b
CH ₃ CH ₃	14.08	13.60 ^c	—	—	—	—
CH ₃ OCH ₃	12.00	12.50 ^d	—	—	—	—

Table 7. Theoretical barrier heights and the experimental activation energy (E_a) for H- abstraction by the ^{*}CH₃ radical from some oxygenated compounds (kcal/mol) at CBS-QB3. ^aRef.⁹⁴, ^bref.⁹⁵, ^cref.⁹⁶, ^dref.⁹⁷.

≥ 1100 K), the Υ channel becomes the main preferable pathway of *n*-butanol oxidation which agrees with previously reported data⁴³. On the other hand, branching ratios of 2ME (Table S12) indicate domination of β H-atom abstraction at the applied temperature range with a remarked competition of ξ H-atom abstraction, especially at higher temperatures. A significant contribution of H-atom abstraction from the O atom of *n*-butanol compared to 2ME at the applied temperatures was observed. Figures 4, 5 depict rate constants (cm³/mol/s) of all abstraction sites of *n*-butanol and 2ME, respectively, versus temperature at CBS-QB3.

Figure 6 displays a comparison of the contribution of similar H-atom abstraction sites from *n*-butanol and 2ME at 200–2000 K. Figure 6a shows a decrease of α H-atom abstraction contribution for the two molecules with rising of temperature, a noticeable decrease of α abstraction contribution for *n*-butanol (from 86% at 200 K to 21% at 2000 K) compared to a moderate decrease for 2ME (from 54.5% at 200 K to 21% at 2000 K). Figure 6b illustrates β channels for the two selected biofuels. For *n*-butanol, the graph indicates a gradual increase in channel contribution with rising of temperature from 1% at 200 K to 21% at 2000 K. However, 2ME has a stable branching contribution with small variation. For the ξ position shown in graph 6c, an increase of contribution of H-atom abstraction is observed for the two molecules with rising of temperature. This channel contributes almost zero at 200 K and rises to 19% and 35% at 2000 K for *n*-butanol and 2ME, respectively. Figure 6d reveals a noticeable high contribution from the alcoholic H-atom abstraction for *n*-butanol compared to that for 2ME. The branching ratio for *n*-butanol shows a maximum at 400 K with 17% which decreases to 9% at 2000 K, while for 2ME, a regular branching ratio increases from zero at 200 K to 5% at 2000 K.

Based on the relation between $\ln(k)$ and $1000/T$ (Figs S1, S2), kinetics of bimolecular oxidation reactions usually adopt non-Arrhenius behavior that fitted to a modified three-parameter Arrhenius relation of A , n , and E_a .

$$k^{\text{TST}} = AT^n e^{-\Delta E_a/RT}$$

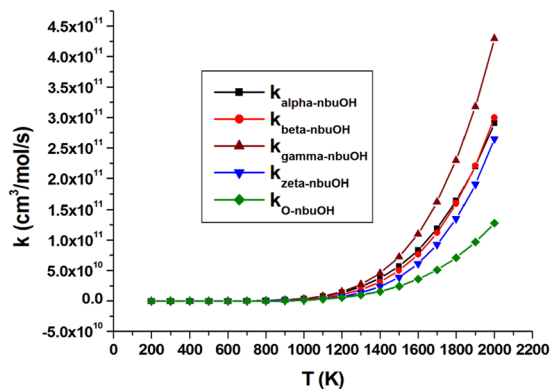


Figure 4. Rate constants ($\text{cm}^3/\text{mol/s}$) of all abstraction sites of *n*-butanol versus temperature change (K).

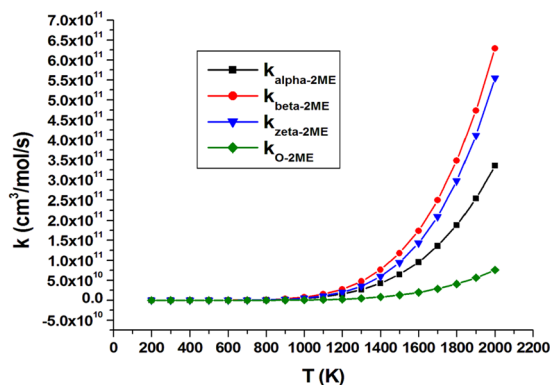


Figure 5. Rate constants ($\text{cm}^3/\text{mol/s}$) of all abstraction sites of 2ME versus temperature change (K).

Table 8 collects rate constants of individual positions and total abstraction rate for *n*-butanol, and 2ME molecules. The results indicate that the calculated rate constant of individual sites and total abstraction of *n*-butanol at CBS-QB3 are in good agreement with those obtained by Katsikidakos *et al.*⁴³. Figure 7 shows a comparison of total abstraction rate constants for 2ME and *n*-butanol at CBS-QB3 which indicates a slightly higher total H-atom abstraction rate for 2ME (four abstraction sites) than that for *n*-butanol (five abstraction sites) as a result of presence of etheric oxygen atom.

Based on Fig. 7, at $T \geq 1300$ K, the total rate for H-abstraction by methyl radical from 2ME was preceded that of *n*-butanol. This can be explained based on the TST Eq. (1) where the rate k^{TST} value is inversely proportional to the $\Delta^\ddagger G^\circ(T)$ value.

Similar to the free energy change equation, the Gibbs energy of the activated complex (transition state) can be obtained from:

$$\Delta^\ddagger G^\circ = \Delta^\ddagger H^\circ - T\Delta^\ddagger S^\circ$$

where $\Delta^\ddagger G^\circ$, $\Delta^\ddagger H^\circ$, and $\Delta^\ddagger S^\circ$ are the transition state standard Gibbs free energy, the standard enthalpy, and the standard entropy, respectively. T is the absolute temperature.

$$\Delta^\ddagger G^\circ = \Delta G_{\text{TS}} - \Delta G_{\text{reactants}}$$

$$\Delta^\ddagger H^\circ = \Delta H_{\text{TS}} - \Delta H_{\text{reactants}}$$

$$\Delta^\ddagger S^\circ = \Delta S_{\text{TS}} - \Delta S_{\text{reactants}}$$

This can be attributed to that the total $\Delta^\ddagger S^\circ(2\text{ME} + \text{CH}_3)$ is more than $\Delta^\ddagger S^\circ(\text{n-butanol} + \text{CH}_3)$ which makes the total $\Delta^\ddagger G^\circ(2\text{ME} + \text{CH}_3)$ less than $\Delta^\ddagger G^\circ(\text{n-butanol} + \text{CH}_3)$.

Summary and Conclusions

The current study describes the main thermodynamic and kinetic features of H-atom abstraction from 2ME by $\bullet\text{CH}_3$ radical based on a comparison with *n*-butanol at the accurate *ab initio* CBS-QB3 methodology. The results can be summarized as follows:

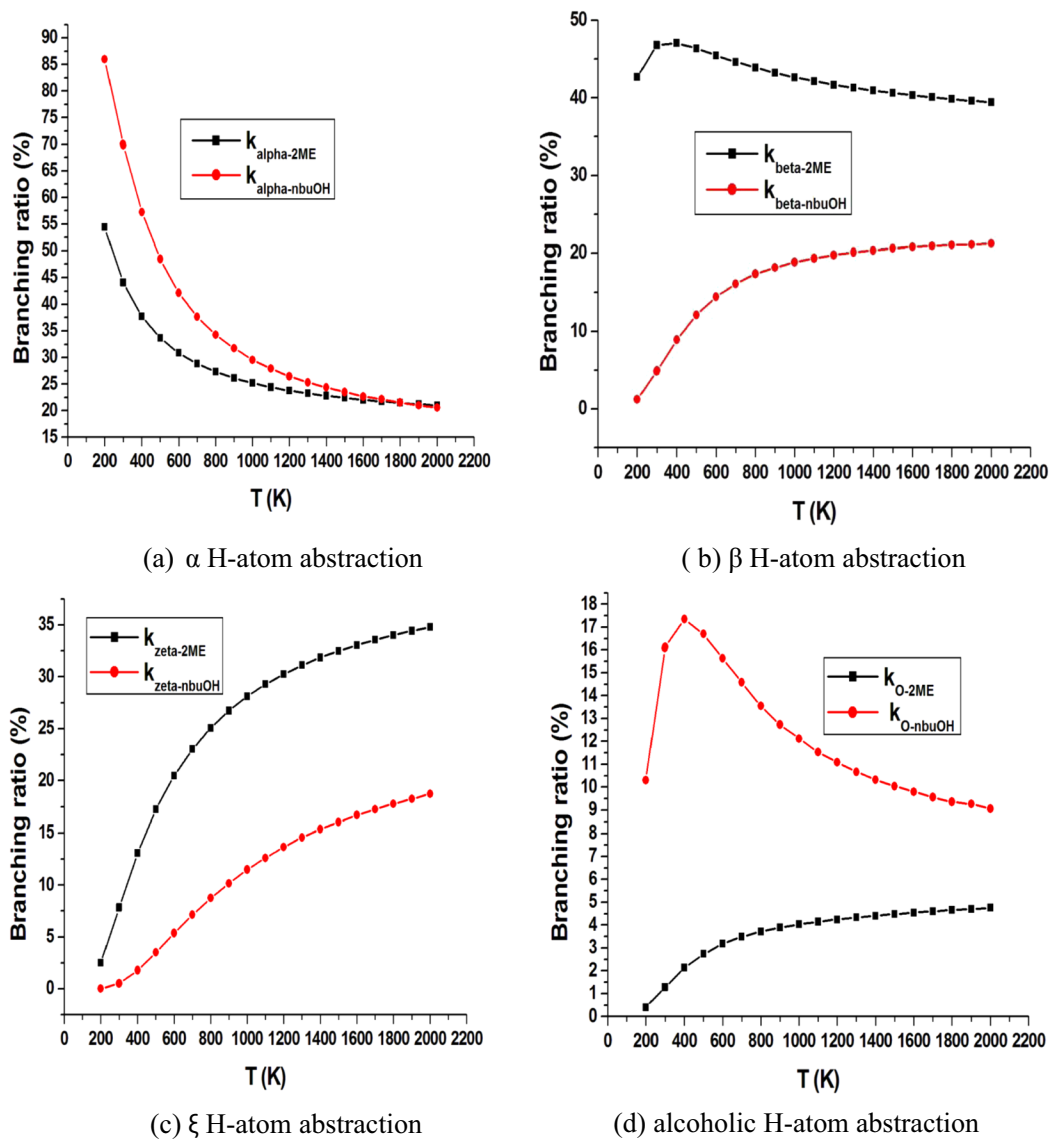


Figure 6. Comparison between temperature dependent branching ratios of H-atom abstraction by methyl radical for *n*-butanol and 2ME at (a) α , (b) β , (c) ξ and (d) alcoholic positions.

Site	2ME	<i>n</i> -butanol
α	$3.09 \times T^{3.586} \exp(-3690/T)$	$2.29 \times T^{3.559} \exp(-3581/T)$
β	$6.36 \times T^{3.587} \exp(-3894/T)$	$2.95 \times T^{3.631} \exp(-4497/T)$
Υ	—	$4.14 \times T^{3.629} \exp(-4431/T)$
ξ	$6.65 \times T^{3.601} \exp(-4457/T)$	$3.78 \times T^{3.630} \exp(-5238/T)$
O	$0.77 \times T^{3.616} \exp(-4343/T)$	$1.60 \times T^{3.552} \exp(-3789/T)$
Total	$7.28 \times T^{3.693} \exp(-3905/T)$	$1.04 \times T^{3.929} \exp(-3847/T)$

Table 8. Modified three- parameter Arrhenius expression ($\text{cm}^3/\text{mol/s}$) for individual sites and total abstraction of 2ME and *n*-butanol at CBS-QB3 over 200–2000 K.

1. There are some agreements between *n*-butanol and 2ME regarding:

- All investigated channels are exothermic except the abstraction of the alcoholic hydrogen atom.
- α H-atom abstraction shows the lowest barrier height among all channels and it represents the highest exothermic route.
- The O-H bond has the highest bond energy.

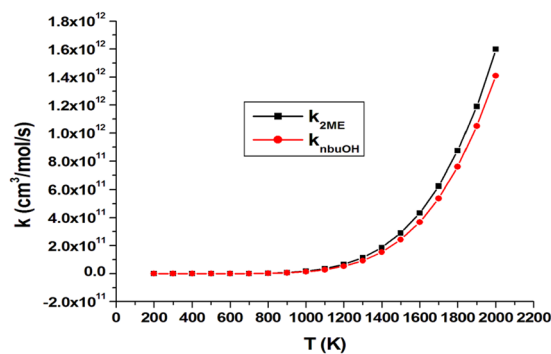


Figure 7. The total rate constant (cm³/mol/s) of 2ME and *n*-butanol over temperature range 200–2000 K.

- The results of barrier heights and reaction energies of 2ME oxidation at CBS-QB3 are in excellent agreement with the corresponding M06-2X values with energy discrepancy less than 1 kcal/mol.
- Energy barriers and reaction energies of 2ME oxidation increase in the order $\alpha < \beta < \Upsilon < O$.
- Replacing Υ CH₂ group in *n*-butanol with etheric oxygen lowers C–H bond dissociation energies for β and ξ hydrogen atoms which enhances oxidation of the bifunctional biofuel compared to the uni-functional one.
- Branching ratio of *n*-butanol indicates domination of the α channel up to 1100 K. Above 1000 K, the Υ channel becomes the main abstraction route. Our study of 2ME oxidation confirms domination of the β channel at the applied temperatures.

Data availability

All data generated through this study are collected in this manuscript and the Supporting Information file.

Received: 13 December 2018; Accepted: 28 September 2019;

Published online: 25 October 2019

References

- Moriarty, P. & Honnery, D. Can renewable energy power the future? *Energy policy*. **93**, 3–7 (2016).
- Panwar, N. L., Kaushik, S. C. & Kothari, S. Role of renewable energy sources in environmental protection: A review. *Renew. Sustain. Energy Rev.* **15**, 1513–1524 (2011).
- Van der Wal, H. *et al.* Production of acetone, butanol, and ethanol from biomass of the green seaweed *Ulva Lactuca*. *Bioresour. Technol.* **128**, 431–437 (2013).
- Ndaba, B., Chiyanzu, I. & Marx, S. *n*-Butanol derived from biochemical and chemical routes: A review. *Biotech. Rep.* **8**, 1–9 (2015).
- Visioli, L. J., Enzweiler, H., Kuhn, R. C., Schwaab, M. & Mutti, M. A. Recent advances on biobutanol production. *Sustain. Chemical Processes*. **2**, 1–9 (2014).
- Jin, C., Yao, M., Liu, H., Lee, C.-F. F. & Ji, J. Progress in the production and application of *n*-butanol as a biofuel. *Renew. Sustain. Energy Rev.* **15**, 4080–4106 (2011).
- Nigam, P. S. & Singh, A. Production of liquid biofuels from renewable resources. *A. Prog. Energy Combust. Sci.* **37**, 52–68 (2011).
- Gua, X. *et al.* Emission characteristics of a spark ignition engine fuelled with gasoline-*n*-butanol blends in combination with EGR. *Fuel*. **93**, 611–617 (2012).
- Black, G., Curran, H. J., Pichon, S., Simmie, J. M. & Zhukov, V. Bio-butanol: combustion properties and detailed chemical kinetic model. *Combust. Flame*. **157**, 363–373 (2010).
- Gu, X., Huang, Z., Li, Q. & Tang, C. Measurements of laminar burning velocities and Markstein lengths of *n*-butanol-air premixed mixtures at elevated temperatures and pressures. *Energy Fuels*. **23**, 4900–4907 (2009).
- Gu, X., Huang, Z., Wu, S. & Li, Q. Laminar burning velocities and flame instabilities of butanol isomers-air mixtures. *Combust. Flame*. **157**, 2318–2325 (2010).
- Yasunaga, K. *et al.* A shock tube and chemical kinetic modeling study of the pyrolysis and oxidation of butanols. *Combust. Flame*. **159**, 2009–2027 (2012).
- Moss, J. T. *et al.* An experimental and kinetic modeling study of the oxidation of the four isomers of butanol. *J. Phys. Chem. A*. **112**, 10843–10855 (2008).
- Dagaut, P., Sarathy, S. M. & Thomson, M. J. A chemical kinetic study of *n*-butanol oxidation at elevated pressure in a jet stirred reactor. *Proc. Combust. Inst.* **32**, 229–237 (2009).
- Sarathy, S. M. *et al.* An experimental and kinetic modeling study of *n*-butanol combustion. *Combust. Flame*. **156**, 852–864 (2009).
- Dagaut, P. & Togbe, C. Experimental and modeling study of the kinetics of oxidation of butanol - *n*-heptane mixtures in a Jet-stirred reactor. *Energy Fuels*. **23**, 3527–3535 (2009).
- Grana, R. *et al.* An experimental and kinetic modeling study of combustion of isomers of butanol. *Combust. Flame*. **157**, 2137–2154 (2010).
- Vasu, S. S., Davidson, D. F., Hanson, R. K. & Golden, D. M. Measurements of the reaction of OH with *n*-butanol at high-temperatures. *Chem. Phys. Lett.* **497**, 26–29 (2010).
- Veloo, P. S., Wang, Y. L., Eglolfopoulos, F. N. & Westbrook, C. K. A comparative experimental and computational study of methanol, ethanol, and *n*-butanol flames. *Combust. Flame*. **157**, 1989–2004 (2010).
- Harper, M. R., Van Geem, K. M., Pyl, S. P., Marin, G. B. & Green, W. H. Comprehensive reaction mechanism for *n*-butanol pyrolysis and combustion. *Combust. Flame*. **158**, 16–41 (2011).
- Weber, B. W., Kumar, K., Zhang, Y. & Sung, C. J. Autoignition of *n*-butanol at elevated pressure and low to intermediate temperature. *Combust. Flame*. **158**, 809–819 (2011).

22. Vranckx, S. *et al.* Role of peroxy chemistry in the high pressure ignition of n-butanol experiments and detailed kinetic modeling. *Combust. Flame*. **158**, 1444–1455 (2011).
23. Sun, J. & Liu, H. Selective hydrogenolysis of biomass-derived xylitol to ethylene glycol and propylene glycol on supported Ru catalysts. *Green Chem.* **13**, 135–142 (2011).
24. Guo, X. *et al.* Conversion of biomass-derived sorbitol to glycols over carbon-materials supported Ru-based catalysts. *Sci. Rep.* **5**, 1–9 (2015).
25. Wang, A. & Zhang, T. One-pot conversion of cellulose to ethylene glycol with multifunctional tungsten-based catalysts. *Acc. Chem. Res.* **46**, 1377–1386 (2013).
26. Liu, Y., Luo, C. & Liu, H. Tungsten trioxide promoted selective conversion of cellulose into propylene glycol and ethylene glycol on a ruthenium catalyst. *Angew. Chem.* **124**, 3303–3307 (2012).
27. Ooms, R. *et al.* Conversion of sugars to ethylene glycol with nickel tungsten carbide in a fed-batch reactor: high productivity and reaction network elucidation. *Green Chem.* **16**, 695–707 (2014).
28. Xiao, Z., Jin, S., Pang, M. & Lianq, C. Conversion of highly concentrated cellulose to 1, 2-propanediol and ethylene glycol over highly efficient CuCr catalysts. *Green Chem.* **15**, 891–895 (2013).
29. Tai, Z. *et al.* Catalytic conversion of cellulose to ethylene glycol over a low-cost binary catalyst of Raney Ni and Tungstic acid. *ChemSusChem*. **6**, 652–658 (2013).
30. Yue, H., Zhao, Y., Ma, X. & Gong, J. Ethylene glycol: properties, synthesis and applications. *Chem. Soc. Rev.* **41**, 4218–4244 (2012).
31. Dagaut, P., Liu, R., Wallington, T. J. & Kurylo, M. J. Kinetic measurements of the gas phase reactions of hydroxyl radicals with hydroxy ethers, hydroxy ketones, and keto ethers. *J. Phys. Chem. A*. **93**, 7838–7840 (1989).
32. Porter, E. *et al.* Kinetic studies on the reactions of hydroxyl radicals with diethers and hydroxyethers. *J. Phys. Chem. A*. **101**, 5770–5775 (1997).
33. Aschmann, S., Martin, P., Tuazon, E. C., Arey, J. & Atkinson, R. Kinetic and product studies of the reaction of selected glycol ether with OH. *Environ. Sci. Technol.* **35**, 4080–4088 (2010).
34. Stemmler, K., Kinnison, D. J. & Kerr, J. A. Room temperature rate coefficients for the reactions of OH radicals with some monoethylene glycol monoalkyl ethers. *J. Phys. Chem.* **100**, 2114–2116 (1996).
35. Galano, A., Idaboy, A. & Ma´rquez, M. F. Mechanism and branching ratios of hydroxyethers + •OH gas phase reactions: relevance of H bond interaction. *J. Phys. Chem. A*. **114**, 7525–7536 (2010).
36. Moc, J. & Simmie, J. M. Hydrogen abstraction from n-butanol by the hydroxyl radical: high-level ab initio study of the relative significance of various abstraction channels and the role of weakly bound intermediates. *J. Phys. Chem. A*. **114**, 5558–5564 (2010).
37. Seal, P., Oyedepo, G. & Truhlar, D. G. Kinetics of the Hydrogen atom abstraction reactions from 1-Butanol by hydroxyl radical: theory matches experiment and more. *J. Phys. Chem. A*. **117**, 275–282 (2013).
38. Zhou, C.-W., Simmie, J. M. & Curran, H. J. Rate constants for hydrogen abstraction by OH from n-Butanol. *Combust. Flame* **158**, 726–731 (2011).
39. Moc, J., Black, G., Simmie, J. M. & Curran, H. J. The unimolecular decomposition and H-abstraction reactions by OH and HO₂ from n-butanol. Computational Methods in Science and Engineering, Advances in Computational Science vol. 2, ed. Simos, T. E. & Maroulis, G. American Inst. of Physics, 161–164 (2009).
40. Zhou, C.-W., Simmie, J. M. & Curran, H. J. Rate constants for hydrogen abstraction by HO₂ from n-Butanol. *Int. J. Chem. Kinet.* **44**, 155–164 (2012).
41. Black, G. & Simmie, J. M. Barrier heights for H-atom abstractions by HO₂ from n-butanol a simple yet exacting test for model chemistries? *J. Comput. Chem.* **31**, 1236–1248 (2010).
42. Katsikidakos, D., Hardalupas, Y., Taylor, A. M. K. P. & Hunt, P. A. Hydrogen abstraction from n-butanol by the methyl radical: high-level ab initio study of abstraction pathways and the importance of low energy rotational conformers. *Phys. Chem. Chem. Phys.* **14**, 9615–9629 (2012).
43. Katsikidakos, D. *et al.* Rate constants of hydrogen abstraction by methyl radical from n-butanol and a comparison of CanTherm, MultiWell and Variflex. *Proc. Combust. Inst.* **34**, 483–491 (2013).
44. Frisch, M. J. *et al.* Gaussian 09; (Gaussian, Inc.: Wallingford, CT, 2009).
45. Zhao, Y. & Truhlar, D. G. The M06 suite of density functionals for main group thermochemistry, thermochemical kinetics, non-covalent interactions, excited states, and transition elements: two new functionals and systematic testing of four M06-class functionals and 12 other functionals. *Theor. Chem. Account.* **120**, 215–241 (2008).
46. Deng, P., Wang, L. & Wang, L. Mechanism of gas-phase ozonolysis of β -myrcene in the atmosphere. *J. Phys. Chem. A*. **122**, 3013–3020 (2018).
47. Dash, M. R. & Rajakumar, B. Theoretical investigations of the gas phase reaction of limonene (C₁₀H₁₆) with OH radical. *Mol. Phys.* **113**, 3202–3215 (2015).
48. Wu, R., Pan, S., Li, Y. & Wang, L. Atmospheric oxidation mechanism of toluene. *J. Phys. Chem. A*. **118**, 4533–4547 (2014).
49. Pan, S. & Wang, L. The atmospheric oxidation mechanism of o-xylene initiated by hydroxyl radicals. *Acta Phys.-Chim. Sin.* **31**, 2259–2268 (2015).
50. Pan, S. & Wang, L. Atmospheric oxidation mechanism of m-xylene initiated by OH radical. *J. Phys. Chem. A*. **118**, 10778–10787 (2014).
51. Montgomery, J. A. Jr., Frisch, M. J., Ochterski, J. W. & Petersson, G. A. A complete basis set model chemistry. VII. Use of density functional geometries and frequencies. *J. Chem. Phys.* **111**, 2822–2827 (1999).
52. Montgomery, J. A. Jr., Frisch, M. J., Ochterski, J. W. & Petersson, G. A. A complete basis set model chemistry. VII. Use of the minimum population localization method. *J. Chem. Phys.* **111**, 6532–6542 (2000).
53. Pokon, E. K., Liptak, M. D., Feldgus, S. & Shields, G. C. Comparison of CBS-QB3, CBS-APNO, and G3 predictions of gas phase deprotonation data. *J. Phys. Chem. A*. **105**, 10483–10487 (2001).
54. Peng, C., Ayala, P. Y., Schlegel, H. B. & Frisch, M. J. Using redundant internal coordinates to optimize equilibrium geometries and transition states. *Comput. Chem.* **17**, 49–56 (1996).
55. Peng, C. & Schlegel, H. B. Combining Synchronous Transit and Quasi-Newton Methods to Find Transition States. *Israel J. Chem.* **33**, 449–454 (1993).
56. Zhurko, G. A. Chemcraft Program V.1.6, <https://www.chemcraftprog.com> (2014).
57. Gonzalez, C. & Schlegel, H. B. An improved algorithm for reaction path following. *J. Chem. Phys.* **90**, 2154–2161 (1989).
58. Gonzalez, C. & Schlegel, H. B. Reaction path following in mass-weighted internal coordinates. *J. Phys. Chem.* **94**, 5523–5527 (1990).
59. Canneaux, S., Bohr, F. & Henon, E. KiSTHELP: a program to predict thermodynamic properties and rate constants from quantum chemistry results. *J. Comput. Chem.* **35**, 82–93 (2014).
60. Steinfeld, J. I., Francisco, J. S. & Hase, W. L. *Chemical kinetics and dynamics*. (Prentice-Hall: Upper Saddle River, NJ, 1999).
61. Wigner, E. Calculation of the rate of elementary association reactions. *J. Chem. Phys.* **5**, 720–725 (1937).
62. Conagin, A., Barbin, D. & Demétrio, C. G. B. Modifications for the Tukey test procedure and evaluation of the power and efficiency of multiple comparison procedures. *Sci. Agric. (Piracicaba, Braz.)* **65**, 428–432 (2008).
63. Moc, J., Simmie, J. M. & Curran, H. J. The elimination of water from conformationally complex alcohol: a computational study of the gas phase dehydration of n-butanol. *J. Mol. Struct.* **928**, 149–157 (2009).
64. Ohno, K., Yoshida, H., Watanabe, H., Fujita, T. & Matsuura, H. Conformational study of 1-butanol by the combined use of vibrational spectroscopy and ab initio molecular orbital Calculations. *J. Phys. Chem.* **98**, 6924–6930 (1994).

65. Vazquez, S., Mosquera, R. A., Rios, M. A. & Alsenoy, C. V. Ab initio-gradient optimized molecular geometry and conformational analysis of 2-methoxyethanol at the 4-21G level. *J. Mol. Struct. (THEOCHEM)*. **188**, 95–104 (1989).
66. El-Nahas, A. M., Mangood, A. H., Takeuchi, H. & Taketsugu, T. Thermal decomposition of 2-butanol as a potential nonfossil fuel: a computational study. *J. Phys. Chem. A*. **115**, 2837–2846 (2011).
67. Thion, S., Zaras, A. M., Szóri, M. & Dagaut, P. Theoretical kinetic study for methyl levulinate: oxidation by OH and CH₃ radicals and further unimolecular decomposition pathways. *Phys. Chem. Chem. Phys.* **17**, 23384–23391 (2015).
68. Hammond, G. S. A correlation of reaction rates. *J. Am. Chem. Soc.* **77**, 334–338 (1955).
69. Rayne, S. & Forest, K. Estimated adiabatic ionization energies for organic compounds using the Gaussian-4 (G4) and W1BD theoretical methods. *J. Chem. Eng. Data* **56**, 350–355 (2011).
70. Lewars, E. G. *Computational Chemistry; Introduction to the Theory and Applications of Molecular and Quantum Mechanics*, third ed. (Springer, 2011).
71. Pedley, J. B. & Rylance, J. *Sussex-NPL Computer Analyzed Thermochemical Data: Organic And Organometallic Compounds*. (University of Sussex: Sussex, U.K., 1977).
72. O'Neal, H. E. & Benson, S. W. In *Free Radicals* (ed. Kochi, J. K.) 275–360 (John Wiley, New York, 1973).
73. Guthrie, J. P. Cyclization of glycol monoesters to give hemiothoesters: a test of the thermochemical method for determining free energies of tetrahedral intermediates. *Can. J. Chem.* **55**, 3562–3574 (1977).
74. Simonetta, M. II problema termico nella catena di reazioni tra ossido di etilene ed alcool metilico. *Chimi. Ind. (Milan)*. **29**, 37–39 (1947).
75. Holmes, J. L. & Lossing, F. P. Ionization energies of homologous organic compounds and correlation with molecular size. *Org. Mass Spectrom.* **26**, 537–541 (1991).
76. Shao, J. D., Baer, T. & Lewis, D. K. Dissociation dynamics of energy-selected ion-dipole complexes. 2. *Butyl alcohol ions*. *J. Phys. Chem.* **92**, 5123–5128 (1988).
77. Bowen, R. D. & Maccoll, A. Low energy, low temperature mass spectra 2—low energy, low temperature mass spectra of some small saturated alcohols and ethers. *Org. Mass Spectrom.* **19**, 379–384 (1984).
78. Cocksey, B. J., Eland, J. H. D. & Danby, C. J. The effect of alkyl substitution on ionisation potential. *J. Chem. Soc. B*, 790–792 (1971).
79. Baker, A. D., Betteridge, D., Kemp, N. R. & Kirby, R. E. Application of photoelectron spectrometry to pesticide analysis. II. Photoelectron spectra of hydroxy-, and halo-alkanes and haloalcohols. *Anal. Chem.* **43**, 375–381 (1971).
80. Katsumata, S., Iwai, T. & Kimura, K. Photoelectron spectra and sum rule consideration. Higher alkyl amines and alcohols. *Bull. Chem. Soc. Jpn.* **46**, 3391–3395 (1973).
81. Watanabe, K., Nakayama, T. & Mottl, J. Ionization potentials of some molecules. *J. Quant. Spectry. Radiative Transfer*. **2**, 369–382 (1962).
82. Benoit, F. M. & Harrison, A. G. Predictive value of proton affinity. Ionization energy correlations involving oxygenated molecules. *J. Am. Chem. Soc.* **99**, 3980–3984 (1977).
83. Peel, J. B. & Willett, G. D. Photoelectron spectroscopic studies of the higher alcohols. *Aust. J. Chem.* **28**, 2357–2364 (1975).
84. Kimura, K., Katsumata, S., Achiba, Y., Yamazaki, T. & Iwata, S., Ionization energies, Ab initio assignments, and valence electronic structure for 200 molecules In *Handbook of HeI Photoelectron Spectra of Fundamental Organic Compounds*, (Japan Scientific Soc. Press, Tokyo, 1981).
85. Williams, J. M. & Hamill, W. H. Ionization potentials of molecules and free radicals and appearance potentials by electron impact in the mass spectrometer. *J. Chem. Phys.* **49**, 4467–4477 (1968).
86. Bartmess, J. E., Scott, J. A. & McIver, R. T. Jr. Scale of acidities in the gas phase from methanol to phenol. *J. Am. Chem. Soc.* **101**, 6046–6056 (1979).
87. Boand, G., Houriet, R. & Baumann, T. The gas phase acidity of aliphatic alcohols. *J. Am. Chem. Soc.* **105**, 2203–2206 (1983).
88. Page, F. M. & Goode, G. C. *Negative Ions and the Magnetron*. 1–156 (Wiley Interscience, London, 1969).
89. Pittam, D. A. & Pilcher, G. Measurements of heats of combustion by flame calorimetry. Part 8- Methane, ethane, propane, n-butane and 2- methylpropane. *J. Chem. Soc. Faraday Trans.* **68**, 2224–2229 (1972).
90. Pilcher, G., Pell, A. S. & Coleman, D. J. Measurements of heats of combustion by flame calorimetry, part 2-dimethyl ether, methyl ethyl ether, methyl n-propyl ether, methyl isopropyl ether. *Trans. Faraday Soc.* **60**, 499–505 (1964).
91. Ohno, K., Imai, K. & Harada, Y. Variations in reactivity of lone-pair electrons due to intramolecular hydrogen bonding as observed by penning ionization electron spectroscopy. *J. Am. Chem. Soc.* **107**, 8078–8082 (1985).
92. Plessis, P. & Marmet, P. Electroionization study of ethane: structures in the ionization and appearance energy curves. *Can. J. Chem.* **65**, 2004–2008 (1987).
93. Butler, J. J., Holland, D. M. P., Parr, A. C. & Stockbauer, R. A threshold photoelectron-photoion coincidence spectrometric study of dimethyl ether (CH₃OCH₃). *Int. J. Mass Spectrom. Ion Processes* **58**, 1–14 (1984).
94. Shannon, T. W. & Harrison, A. G. The reaction of methyl radicals with methyl alcohol. *Can. J. Chem.* **41**, 2455–2461 (1963).
95. Gray, P. & Herod, A. A. Methyl radical reactions with ethanol and deuterated ethanols. *Trans. Faraday Soc.* **64**, 1568–1576 (1968).
96. Moller, W., Mozzhukhin, E. & Wagner, H. Gg. High temperature reactions of CH₃. 2. H-abstraction from alkanes. *Ber. Bunsenges. Phys. Chem.* **91**, 660–666 (1987).
97. Hidaka, Y., Sato, K. & Yamane, M. High-temperature pyrolysis of dimethyl ether in shock waves. *Combust. Flame* **123**, 1–22 (2000).

Author contributions

M.A. Abdel-Rahman prepared figures and tables and first draft of the paper. T.M. El-Gogary, N. Al-Hashimi, M.F. Shibl, K. Yoshizawa, and A.M. El-Nahas supervised M.A. Abdel-Rahman. They gathered everything, checked the data, discussed it and digested it in the final version of the manuscript.

Competing interests

The authors declare no competing interests.

Additional information

Supplementary information is available for this paper at <https://doi.org/10.1038/s41598-019-51544-8>.

Correspondence and requests for materials should be addressed to N.A. or A.M.E.

Reprints and permissions information is available at www.nature.com/reprints.

Publisher's note Springer Nature remains neutral with regard to jurisdictional claims in published maps and institutional affiliations.



Open Access This article is licensed under a Creative Commons Attribution 4.0 International License, which permits use, sharing, adaptation, distribution and reproduction in any medium or format, as long as you give appropriate credit to the original author(s) and the source, provide a link to the Creative Commons license, and indicate if changes were made. The images or other third party material in this article are included in the article's Creative Commons license, unless indicated otherwise in a credit line to the material. If material is not included in the article's Creative Commons license and your intended use is not permitted by statutory regulation or exceeds the permitted use, you will need to obtain permission directly from the copyright holder. To view a copy of this license, visit <http://creativecommons.org/licenses/by/4.0/>.

© The Author(s) 2019